

A Distributed Model of Ionomeric Polymer Metal Composite

A. Punning*, U. Johanson, M. Anton, A.Aabloo, M.Kruusmaa
Institute of Technology, Tartu University, Nooruse 1, Tartu 50411, Estonia

ABSTRACT: This paper presents a novel model of an IPMC (Ionomeric polymer metal composite). An IPMC is modeled as a lossy RC distributed line. Unlike other electromechanical models of an IPMC, the distributed nature of our model permits modelling the non-uniform bending of the material. Instead of modeling the tip deflection or uniform deformation of the material, we model the changing curvature. The transient behavior of the electrical signals as well as the transient bending of the IPMC are described by Partial Differential Equations. By implementing the proper initial and boundary conditions we develop the analytical description of the possibly nonuniform transient behavior of an IPMC consistent with the experimental results.

Keywords: IPMC, distributed RC lines

1. INTRODUCTION

IPMCs are materials that bend in electric field (Figure 1). An IPMC actuator consists of a highly swollen polymer sheet, such as Nafion™, filled with water or ionic liquid and plated with metal on both sides. Applied voltage causes the migration of ions inside the polymer matrix which in turn causes the non-uniform distribution of the ions inside the polymer. As a result, the polymer sheet bends. The direction of bending depends on the polarity of the applied voltage. An overview of the working principle of IPMC actuators can be found e.g. in (Shahinpoor, 2003).

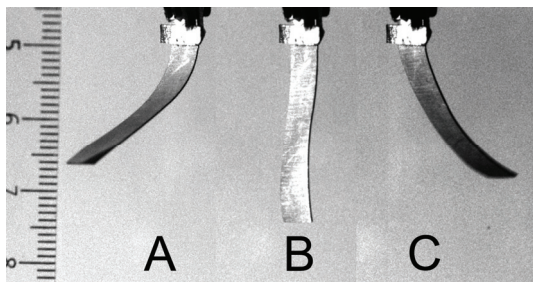


Figure 1. An IPMC sheet in a bent configuration with the opposite driving voltage polarities (A and C) and an initial configuration with no electric stimulus applied (B).

IPMC actuators and sensors have many appealing properties from the implementation point of view. Being noiseless, soft and flexible, mechanically simple, lightweight and resilient they have potentially many applications in the areas of noise damping, haptics, smart textiles, biorobotics, medicine, space applications and elsewhere (Shahinpoor and Kim, 2005).

The state-of-the-art of the IPMC sensor and actuator technology is not thoroughly understood which makes it difficult to predict the behavior of this material and therefore limits the potential applications areas.

Several models are proposed so far to model the behavior of IPMC sensors and actuators. A systemized overview of the existing models can be found in (Kothera, 2005). The most accurate IPMC models are derived from first principles and comprise the modeling of underlying electrochemical phenomena coupled to the mechanical bending of the sheet (Nemat-Nasser and Thomas, 2004; Asaka and Oguro, 2000; Tadokoro et al., 2004). While capturing the complex phenomena inside the IPMC actuator those models tend to be complex, computationally time consuming and require laborious parameter identification.

The empirical models describing the behavior of the actuator on a macro-level are derived experimentally by curve fitting (Mallavarapu and Leo, 2001; Kanno et al. 1995) or based on the description of some sort of an equivalent circuit (Kanno et al. 1996; Bonomo et al. 2007; Newbury and Leo 2003). Kanno et al. (1996) have proposed a model in a form of an RC-line but by representing the circuit in a form of a first order transfer function they reduce it to a lumped model and define the relationship between tensile stress and input current. Also the model proposed by Bao et al. (2002) is based on the assumption of uniform properties but it is recognized that the distributed model would provide a more accurate description. Yim et al. (2006) propose a distributed model, where the IPMC actuator is divided to segments, but each

segment is assumed to be driven separately to achieve waving motion of the actuator and each segment is again treated as a lumped model subject to uniform tensile forces.

The models proposed so far can model the tip displacement or output force of the tip but not the configuration of the entire actuator surface. The model proposed by us is different in the sense that it takes into consideration the fact that deformation of the IPMC material is non-uniform. Figures 1 and 2 represent a typical behavior of the actuator where the bending curvature from the electric contacts along the sheet decreases.

In this paper we propose modelling the IPMC actuator as a distributed RC line. This presentation permits identifying the electric current through the polymer matrix at every point of the IPMC sheet. As such, it corresponds more accurately to the real situation where the bending curvature of the actuator at each point is determined by the migration of ions at that particular location. The variations in the ion concentration cause non-uniform bending.

We represent the model of an IPMC actuator in an analytical and simulated form based on the theory of RC transmission lines and show the solution in case of the step input voltage. By coupling the current through the polymer matrix to the mechanical bending of the actuator we derive the electromechanical model of an IPMC. We then proceed by representing the simulation results and thereafter demonstrate that these results are well consistent with the experimental data obtained from the experiments of three different types of IPMC.

2. CHARACTERIZATION OF THE ACTUATOR.

Generally the models of an IPMC described in the literature do not characterize the shape of IPMC-based devices. They usually describe only the motion of the tip or the bending radius of the device assuming that the bending radius is constant. The equipment used to characterize these parameters are for instance laser position sensors or force gauges (Jung et al. 2003, Richardson et al. 2003, Bandopadhyaya et al. 2006).

In order to observe the mechanical motion of the actuator, we developed a new methodology that permits describing the flexure of an IPMC. It is a computer vision system consisting of a fast CCD camera and a PC with image

processing software. The National Instruments Vision was used for both frame grabbing and image processing. The direction of the camera is set transverse to the actuator and the experiment is illuminated from the background through a frosted glass. In perfect conditions the image of the actuator recorded in such a way consists of a single contrast curved line. It is easy to use image processing software to process the shape of the actuator during each particular frame. The separate frames of a bending actuator, recorded in such a way, are depicted in Figure 2.

It is apparent from Figure 2., that in the beginning of the input pulse (images 0...0.4s in Figure 2.-A) the actuator performs a sharp motion close to the input contacts only, the free end remains almost straight.

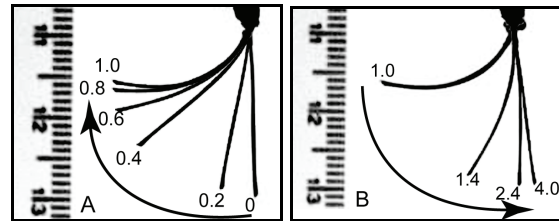


Figure 2. Overlay of a series of frames showing the response of an actuator to a 1s driving voltage pulse. A – actuation during the pulse; B – relaxation after the pulse. The numeric characters indicate the time instant of the frame.

Later (images 0.4...1.0s in Figure 2.-A) the flexure of the actuator propagates gradually on, but the flexure at the region close to the contacts does not increase any more. During the relaxation (images 1.0...4.0s in Figure 2.-B) the sharp decrease of the flexure takes place close to the input contacts again, whereas the remaining part of the actuator straightens slowly in few seconds.

The voltages drop along the electrodes of the actuator can be recorded by attaching additional terminals to its surface. The outline of the experimental setup for electrical measurements is depicted in Figure 3.

We measure the voltage distribution on the surface of a working IPMC-based actuator or sensor by attaching a set of pairs of lightweight contacts to its surface using special lightweight clips, and connect them via thin wires to the measuring equipment. Voltages U_C , U_D , U_E and U_F with respect to the ground are measured at the contacts C, D, E and F respectively. The input voltage U_A is measured at the contact A.

The voltages between the two faces of the sample can be calculated as $U_C - U_D$, and $U_E - U_F$.

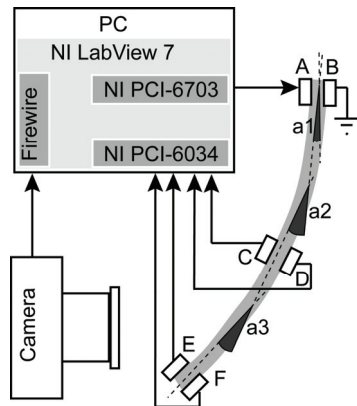


Figure 3. Setup for electrical measurements.

The voltages measured on an actuator, bending similarly to the one presented in Figure 2, are represented as a 3D graph in Figure 4.

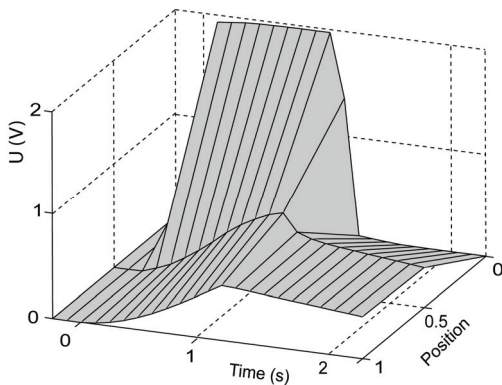


Figure 4. Voltages along a bending actuator.

It is apparent from Figure 4 that even in the middle of the sample the voltage does not reach a substantial value. The voltage at the free end only slightly differs from the voltage in the middle.

In order to describe the bending movement of the actuator, the image of the bending sheet is divided into segments assumed to have a constant curvature. The principle of determining the angles is shown in Figure 3. (angles $a_1 - a_3$). The angles of the segments are calculated from each frame of the video. The changing flexure of the actuator, electrically characterized in Figure 4, is depicted in Figure 5. It can be observed that the bending of the sheet is faster and stronger close to the input contacts, getting progressively weaker as well as delayed towards the free end of the sheet.

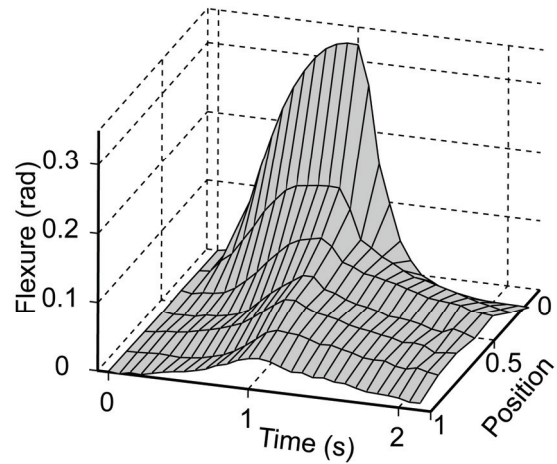


Figure 5. Mechanical response of an actuator to a step input voltage. The "Position" axis stands for the relative coordinate starting from the input contacts.

It is apparent that the two graphs – the graph of voltages versus position and time, and the graph of bending angles versus position and time - are similar. The characteristic behavior of both voltage and flexure is delayed and progressively weakening, with the maximum near the input contacts.

3. A DISTRIBUTED MODEL OF IPMC.

The fact that the electrical perturbation as well as the change of the flexure spreading along the actuator at finite speed and the fact that the flexure and voltage along the surface behave similarly were the motivations to develop a distributed model of an IPMC.

The basis of the model is the distributed model of an IPMC proposed by Kanno et al. (1996). Originally Kanno divided a piece of an IPMC into ten similar segments and modelled the relation between the input current and the tip displacement. Dividing the same piece into an infinite number of infinitesimally short similar segments, gives an RC transmission line. The resulting distributed RC line represented by a series of equivalent circuits with discrete elements is shown in Figure 6. The transient behavior of electrical signals, for instance voltage, electric current, charge, etc. along this kind of lines can be described by Partial Differential Equations (PDE) with the proper initial and boundary conditions.

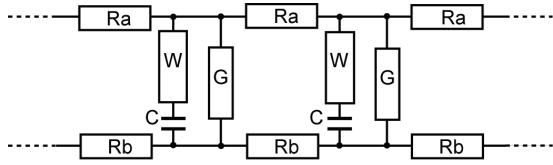


Figure 6. The distributed RC line describing an IPMC, represented by a series of equivalent circuits with discrete elements.

The distributed model of an IPMC represented by an infinite series equivalent circuits with discrete elements of infinitesimally short single units is given in Figure 7. The conductivity of the electrodes of an IPMC is represented by a series of resistances of the opposite electrodes Ra and Rb , connecting the single units. Each single unit contains the electrical parameters determining the propagation of voltage along the transmission line and the elements for calculating the mechanical behavior of the actuator within the limits of that unit.

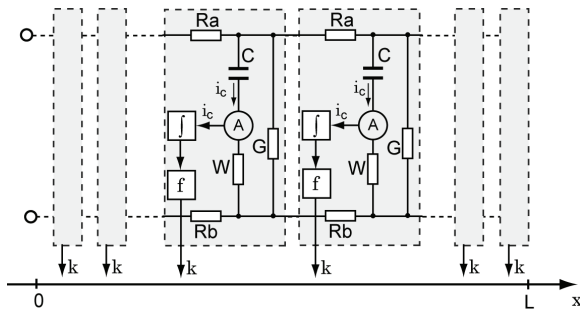


Figure 7. The distributed model of an IPMC.

There are two fundamental causes of the electric current between the electrodes of an IPMC through the polymer matrix:

1. The current caused by ionic conductivity. Relocating ions constitute the pseudocapacitance of the double-layer which forms at the interface between the ion exchange membrane and the metal electrode (Sadeghipour et al. 1992). As described above, the resulting irregular density of hydrated ions is the cause of bending of the IPMC. The resulting deformation of the IPMC is proportional to the total amount of relocated ions. In the equivalent circuit the pseudocapacitance is modeled by shunt capacitors C between the electrodes in each unit. The conductivity W denotes the summarized transversal ionic conductivity of the electrodes and the ionomer.
2. The current caused by electrochemical electrode reactions, for example electrolysis of the solvent. The electrode reactions appear

only if the voltage between the electrodes exceeds some certain critical level, depending on the materials used. The electrode reactions consume energy and affect the propagation of voltage, but do not have a direct effect on the deformation of the IPMC. In the equivalent circuit the electrode reactions are represented as shunt resistors G between the electrodes in each single unit.

The electric charge q determines the mechanical flexure k within the limits of the single unit. As the electric charge can be expressed as the derivative of the current with respect of time, the total electric charge q carried over within each unit is calculated as an integral of current i_C . Figuratively, each single unit of the RC distributed line contains a block composed of an ammeter, measuring current i_C

through the capacitance C , an integrator in order to determine the charge moved over within the limits of that unit, and function f describing the bending effect of a charge, moving to the electrode. In the simplest case the flexure is proportional to the charge and the block f contains

$$k = \Upsilon q, \quad (1)$$

where Υ is the coefficient for the bending effect of the charge.

4. THE ANALYTICAL EQUATIONS DESCRIBING THE DISTRIBUTED MODEL OF AN IPMC

When the input current is applied through one end of a circuit as shown in Figures 6 or 7, the current flows through $C - W$ and G of the whole chain. According to Ohm's Law, the current induces voltage drops on the resistances Ra and Rb and the voltage across the line diminishes until the circuit reaches an equilibrium state. In the course of charging of the capacitive elements C the voltages and currents change, but at every time instant the system stays in its equilibrium state. This transient behavior can be described by PDE-s.

The step response of a system is the output of the system when a unit step function is used as the input and it is a common analysis tool used to determine certain metrics about a system. As we show hereinafter, the step response of the distributed line depicted in Figure 6 is solvable

in an analytical form. On the other hand it is easy to verify the theoretical model by applying the step voltage to the input of the IPMC actuators, describing their electromechanical response and measuring the transient behavior of the electrical parameters.

In this section we give the equations describing the transient behavior of the voltage $u(x,t)$ for the distributed line of the finite length L depicted in Figure 6. when a voltage step is applied to its input. The derivation of the PDE and the procedure of applying the initial and boundary conditions is described in detail in (Punning and Jalviste, 2009) and is based on the solution of the heat equation with different boundary conditions (Powers, 2006; Kreyszig, 2006). We give only the short overview and the relevant equations in the current paper. From the analytical solution describing the transient behavior of voltage we derive the transient behavior of the charge $q(x,t)$ of the capacitive element C , actually determining the amount of bending of IPMC, for example in the simplest case following the equation (1).

First, we transfer the line shown in Figure 6 into the *Cauer canonical form* (Szekely, 2003) by replacing the two resistances Ra and Rb by their sum $R = Ra + Rb$. The resulting line is depicted in Figure 8.

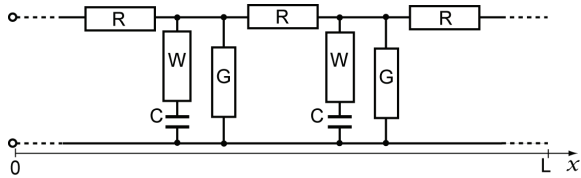


Figure 8. The Cauer canonical form of the line represented in Fig. 6.

As shown in Figure 9, the parameters R and C are the resistance of the conductive layer and the capacitance of the dielectric per unit length of the line, respectively. The loss parameters W and G are the transversal conductivities per unit length along the line. For visual clarity in Figure 9 the parameters R, C, G , and W , all defined per unit length along the coordinate x , are represented as discrete elements of a single cell of the line. The voltage checkpoints and the selected positive directions of the currents are indicated by arrows. We assume that all these parameters are uniform and time-invariant. Voltages and currents are assumed to be functions of the distance along the line and time,

i.e. $i \equiv i(x,t)$, $i_C \equiv i_C(x,t)$, $i_G \equiv i_G(x,t)$, $u \equiv u(x,t)$, and $u_C \equiv u_C(x,t)$.

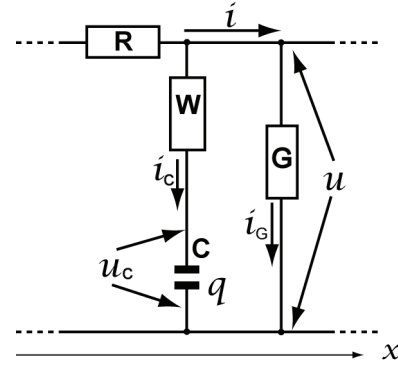


Figure 9. The meaning of the line parameters, voltages and currents for the distributed line.

In the next sections we give the equations describing the behavior of voltage, charge, water carried over and the bending radius.

4.1. The behavior of voltage

The variation of current along the coordinate x at instant t is equal to the sum current through the chains “ $C - W$ ” and “ G ”:

$$\frac{\partial}{\partial x} i(x,t) = -(i_C(x,t) + i_G(x,t)), \quad (2)$$

where

$$i_G(x,t) = Gu(x,t). \quad (3)$$

The variation of voltage along the coordinate x is equal to the voltage drop on resistance- R :

$$\frac{\partial}{\partial x} u(x,t) = -Ri(x,t). \quad (4)$$

Current $i_C(x,t)$ charging the capacitance C is given by

$$i_C(x,t) = C \frac{\partial}{\partial t} u_C(x,t). \quad (5)$$

Voltages in the chain $C - W$ add up to the line voltage:

$$u(x,t) = u_C(x,t) + \frac{1}{W} i_C(x,t). \quad (6)$$

We now have 4 equations with 4 unknown variables: $i(x,t)$, $i_C(x,t)$, $u_C(x,t)$ and $u(x,t)$. After some substitutions and rearrangements we get the PDE describing the transient behavior of voltage $u(x,t)$ along the line in the form

$$\frac{\partial^3}{\partial x^2 \partial t} u(x,t) + \frac{W}{C} \frac{\partial^2}{\partial x^2} u(x,t) - R(W+G) \frac{\partial}{\partial t} u(x,t) - \frac{RGW}{C} u(x,t) = 0. \quad (7)$$

This equation can be easily solved by a method called the separation of variables. The general solution of the PDE (7) for $u(x,t)$ is

$$u(x,t) = (A \sin(\omega x) + B \cos(\omega x)) e^{-\frac{W(\omega^2 + RG)}{C(\omega^2 + RG + RW)} t}, \quad (8)$$

where A and B are arbitrary constants, with values determined from the boundary conditions.

Next, we introduce the term „steady voltage distribution”. After a long time ($t \rightarrow \infty$) under a constant input voltage the capacitance C finally charges completely and the voltages $u(x,t)$ and $u_C(x,t)$ are equalized, $u(x) = u_C(x)$. As it can be inferred from Figures 8 9, the steady current through the distributed resistive network, formed by R and G , still remains. This results in a diminishing steady voltage, denoted by $u_{ST}(x)$, along the line. The equation describing the steady voltage distribution is

$$\frac{\partial^2}{\partial x^2} u_{ST}(x) = RG u_{ST}(x). \quad (9)$$

By applying the condition of the input voltage U at $x=0$: $u_{ST}(0) = U$, and the open end condition, $i_{ST}(L) = 0$ or $\frac{\partial}{\partial x} u_{ST}(L) = 0$, to its general solution $u_{ST}(x) = A e^{\sqrt{RG}x} + B e^{-\sqrt{RG}x}$, we find that

$$u_{ST}(x) = U \frac{\cosh(\sqrt{RG}(x-L))}{\cosh(\sqrt{RGL})}. \quad (10)$$

It is self-evident that when the input of the initially charged line is shorted, the capacitance C finally discharges through the resistive network and the shorted input, and the steady voltage is zero: $u_{ST}(x) = 0$.

The initial/boundary conditions can be applied to the equation (8) using the method of Fourier series. This procedure is thoroughly described in (Punning and Jalviste, 2009). Naturally, it is possible to define many different initial/boundary conditions to (8), that result in an analytical solution. In the current paper we describe only two distinct cases of practical importance:

A) the step voltage with amplitude normalized to 1 is applied to the input of the initially discharged line. The initial and boundary conditions for this case are:

- initial voltage distribution: $u(x,0)=0$
- input voltage at $x=0$: $u(0,t) = 1$
- open end condition: $\frac{\partial}{\partial x} u(L,t)=0$
- steady voltage distribution:

$$u_{ST}(x) = \frac{\cosh(\sqrt{RG}(x-L))}{\cosh(\sqrt{RGL})}$$

B) the shorted input of the line that has been under the input of voltage of amplitude of 1 unit until the steady distribution is formed. The initial and boundary conditions for this case are:

- initial voltage distribution:

$$u(x,0) = \frac{\cosh(\sqrt{RG}(x-L))}{\cosh(\sqrt{RGL})}$$

- input voltage at $x=0$: $u(0,t) = 0$
- open end condition: $\frac{\partial}{\partial x} u(L,t)=0$
- steady voltage distribution: $u_{ST}(x)=0$

In general, the voltage-step response of the distributed lines of length L depicted in Figure 8- can be expressed as

$$u(x,t) = U \sum_{n=1}^{\infty} (b_n \varphi(\omega_n x) e^{-k_n t}) + u_{ST}(x), \quad (11)$$

where

$$k_n = \frac{W(\omega_n^2 + RG)}{C(\omega_n^2 + RG + RW)}, \quad (12)$$

and where $\varphi(\omega_n, x)$, ω_n , b_n , and $u_{ST}(x)$ are the eigenfunctions, eigenvalues, Fourier coefficients, and the steady voltage distribution respectively. All these quantities depend on the initial/boundary conditions. Applying the boundary conditions for our two cases, we get that the solutions for voltage are:

$$\text{A) } u(x,t) = \sum_{n=1}^{\infty} \left(-b_n \sin\left(\frac{2n-1}{2L} \pi x\right) e^{-k_n t} \right) + \frac{\cosh(\sqrt{RG}(x-L))}{\cosh(\sqrt{RGL})} \quad (13)$$

$$\text{B) } u(x,t) = \sum_{n=1}^{\infty} \left(b_n \sin\left(\frac{2n-1}{2L} \pi x\right) e^{-k_n t} \right) \quad (14)$$

where

$$k_n = \frac{W(4RGL^2 + \pi^2(2n-1)^2)}{C(\pi^2(2n-1)^2 + 4RL^2(G+W))} \quad (15)$$

and

$$b_n = \frac{4\pi(2n-1)}{\pi^2(2n-1)^2 + 4RGL^2}. \quad (16)$$

4.2. The behavior of charge

As described above, the mechanical flexure of the actuator $k(x,t)$ is determined by the transitory charge $q(x,t)$ of the capacitance C . The PDE describing the behavior of the charge can be derived similar to the derivation of the PDE for voltage in the previous section. Using the relation describing that the current through the capacitor is the derivative of its charge by time

$$i_C(x,t) = \frac{\partial}{\partial t} q(x,t) \quad (17)$$

and the relation between the charge and voltage of a capacitor

$$u_C(x,t) = \frac{1}{C} q(x,t), \quad (18)$$

it is possible to convert the equations (2)-(6) to 4 new equations with 4 unknown variables:

$i(x,t)$, $i_C(x,t)$, $q(x,t)$ and $u(x,t)$. From

these equations it is easy to derive the PDE describing the behavior of the charge $q(x,t)$:

$$\frac{\partial^3}{\partial x^2 \partial t} q(x,t) + \frac{W}{C} \frac{\partial^2}{\partial x^2} q(x,t) - R(W+G) \frac{\partial}{\partial t} q(x,t) - \frac{RGW}{C} q(x,t) = 0. \quad (19)$$

It is intriguing that the PDE-s describing the behavior of voltage (7) and the charge (19) are exactly similar. The only difference between these two is in the initial and boundary conditions. The general solution for the charge $q(x,t)$ is similar to (8):

$$q(x,t) = (A \sin(\omega x) + B \cos(\omega x)) e^{-\frac{W(\omega^2 + RG)}{C(\omega^2 + RG + RW)} t}. \quad (20)$$

Nevertheless it is not possible to apply the initial/boundary conditions to (20) using the method of separation of the variables, because the charge $q(0)$ at the boundary $x=0$ is not a constant but some unknown time-dependent function.

Instead, we derive the behavior of the charge $q(x,t)$ from the equation (6). Using the relations (17) and (18), we can write

$$u(x,t) = \frac{1}{C} q(x,t) + \frac{1}{W} \frac{\partial}{\partial t} q(x,t). \quad (21)$$

Solving (21) for $q(x,t)$ gives

$$q(x,t) = \left(\int_0^t W u(x,\tau) e^{\frac{W}{C}\tau} d\tau + \rho(x) \right) e^{-\frac{W}{C}t}, \quad (22)$$

where $\rho(x)$ is the constant of integration. From the boundary conditions we can find that $\rho(x)$ equals to the initial distribution of charge corresponding to the initial voltage distribution at $t=0$. For the case A) the initial distribution of charge is self-evidently zero: $\rho(x)=0$. For the case B) the initial charge $q_{ST}(x)$ can be found from the final steady voltage distribution of case A) as

$$\rho(x) = C u_{ST}(x), \quad (23)$$

where $u_{ST}(x)$ is defined by (10).

After substituting the behavior of voltage described by (13) or (14) and the corresponding steady charge distribution into (22) we get the behavior of the charge $q(x,t)$ along the line for our two cases.

4.3. Hydraulic pressure

The bending movement of an IPMC is produced by the hydraulic pressure caused by the moving hydrated charge. In the simplest case the amount of water carried over by the migrating cations is proportional to the charge:

$$k(x,t) = \Upsilon q(x,t), \quad (24)$$

where Υ is the coefficient of hydratization of the cations.

Several authors have described the slow back-relaxation of the IPMC actuators after the quick response to the applied voltage (Bao et al. 2002; Shahinpoor, 2003). This phenomenon is explained with the water leakage resulting from a high-pressure layer near the cathode toward to the anode through channels in the polymer backbone. The research of relaxation effect and the development of the equations for the hydraulic pressure considering the back-relaxation, suitable for the distributed model of an IPMC, is the subject of our future work.

4.4. Bending radius

The derivation of the relation between the curvature of the swollen polymer matrix and the charge carried over is described in Berry and Pritchett, 1984). The equations are derived

similar to those employed by Timoshenko in his work on bi-metallic strips (Timoshenko, 1925). Actually Berry and Pritchett describe the method of determining the coefficient of moisture swelling of polymers by their bending curvature. In our PMC model we use the result conversely – we determine the bending curvature from the nonuniform concentration profile of liquid inside the polymer.

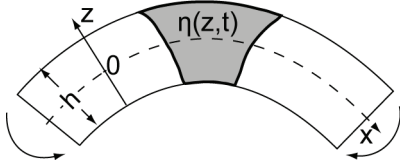


Figure 10. Self-induced bending of a polymer strip caused by the water concentration profile $\eta(z,t)$ through the polymer layer.

Assuming that the polymer is isotropic and swells in volume V proportionally to a uniform water concentration η_0 , we may write

$$\varepsilon = K\eta_0, \quad (25)$$

where ε is a hygroscopic strain analogous to a thermal expansion strain of bi-metal thermostats, and K is a linear swelling parameter equal to one-third of the volumetric swelling factor:

$$K = \eta_0 \frac{1}{3} \frac{\Delta V}{V}. \quad (26)$$

A nonuniform concentration profile of water $\eta(z,t)$ through the across the IPMC (z -coordinate) of the strip will cause elongation, bending and internal stress. With the assumption that plane cross-sections remain planar, the stress $\sigma(z,t)$ is given by

$$\frac{\sigma(z,t)}{E_1} = K\eta(z,t) - \varepsilon_0(t) - \frac{z}{r(t)}, \quad (27)$$

where E_1 denotes $\frac{E}{(1-\nu)}$, E and ν are

Young's modulus and Poisson ratio of the polymer layer, $\varepsilon_0(t)$ is the strain at midplane

$z = 0$, and $r(t)$ is the radius of curvature. Since the polymer layer is under no external forces, we can write

$$\frac{1}{r(t)} = \frac{12K}{h} \int_{-1/2}^{1/2} \eta(s,t) ds, \quad (28)$$

where we introduced the dimensionless coordinate $s = \frac{z}{h}$ for convenience.

Assuming that the concentration profile of water along the z -coordinate of the strip is linear: $\eta(x,s,t) = s\mu(x,t)$, the equation (28) reduces to

$$r(x,t) = \frac{h}{K\mu(x,t)}. \quad (29)$$

4.5. The behavior of electric current

The distribution of electric current between the surface electrodes cannot be measured directly from an IPMC sample. Nevertheless, it can be derived from the previous equations. As described in Section 3, it can analysed by its components depending on its effect to the bending motion. The current caused by ionic conductivity $i_C(x,t)$, described by (17), is related to the behavior of charge $q(x,t)$, actually producing the movement. The current caused by electrochemical electrode reactions $i_G(x,t)$, described by (3), only consumes energy but does not cause the bending motion. Both components of the current participate in determining of the distribution of voltage and the charge and hence, the bending movement of the actuator.

The total input current $i_{in}(t)$ of the sample is determined by all currents over the full length of the distributed line:

$$i_{in}(t) = \int_0^L (i_C(x,t) + i_G(x,t)) dx. \quad (30)$$

5. ESTIMATION OF THE PARAMETERS

The values of the resistances of the surface electrodes of an IPMC can be measured using a four-probe system. This method eliminates inexactnesses caused by the inconsistent current density and the resistances of the contacts.

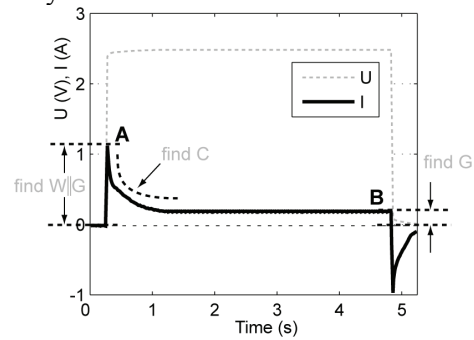


Figure 11. Response of the electric current to a rectangular voltage pulse.

The values of the parameters G , W and C can be determined using a technique with voltage step pulses as follows. A small piece of an IPMC material is fixed between contact clamps made of gold so that the whole piece of the measured material is covered with the contacts. In this configuration the resistance of the electrodes does not influence the results. The typical response of electric current corresponding to a long-lasting step voltage input is depicted in Figure 11. Electric current peaks sharply at the very first moment (instant A). After charging the whole pseudocapacitor, electric current remains at a stable level (instant B).

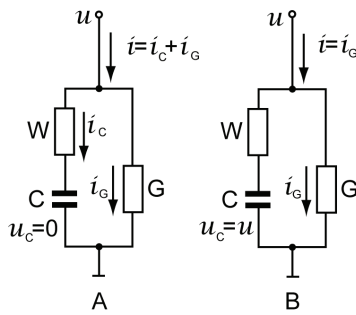


Figure 12. Estimation of the resistances G and W .

This behaviour of current can be explained by analysing the equivalent circuit illustrated in Fig. 12. At the very first moment, when the capacitor C is totally discharged, the current flows through the parallel resistances G and W (instant A). When the capacitance C is totally charged, the current flows through resistance G only (instant B). The capacitance C can be found from the decay of the electric current.

6. VERIFICATION OF THE MODEL

In order to prove the validity of the distributed model of the IPMC, we present the actual behavior of different IPMC actuators and the computational results of the simulations using the equations given above. First we compare the behavior of the two fundamentally different IPMC materials, then the actuators made of the same material, but having different dimensions.

6.1. Behavior of actuators with different electrical parameters

The experiments show that the electromechanical responses of the different types of IPMCs are different. Some materials bend faster, some slower; some have almost

constant bending radius, some bend non-uniformly. In order to demonstrate the validity of the distributed model of the IPMC for different materials, we compare the results of the experiments carried out with two fundamentally different IPMC materials manufactured by us and the simulations of the distributed model of the IPMC using the estimated parameters. We give the parameters of the samples of both measured materials using the methodology described in Section 5, and present the graphs of voltage and bending movement as described in Section 2. Simultaneously we simulate the same graphs by the equations given in Section 4 using the measured parameters and compare the measured and simulated behaviors of the samples.

We used the following IPMC samples for experimental validation:

Sample1 - an IPMC covered with platinum electrodes using the method of electroless deposition;

Sample2 - an IPMC covered with gold electrodes using the direct assembly method.

The parameters of the samples, measured using the methodology described in Section 5, are given in Table1.

The *Sample1* is made of 0.25 mm thick Nafion membrane and covered with thin platinum electrodes using the method of electroless deposition. It is a water-containing IPMC, intended to work in a wet environment. The cations introduced to the ionomer were Li^+ . This material is thick, hence more stiff than the other material. The thicker material contains potentially more cations, thus it has a relatively large pseudocapacitance. The resistance of the electrodes of this sample is rather high, but still good enough to ensure conductivity. The nonuniform behavior of this sample is considerable due to the high resistance of the electrodes. The value of the conductivity W (see Figure 7) is relatively high. When the applied voltage is lower than the voltage required for the electrolysis of water, the value of G is very low - in the range of about $10^{-4} \frac{1}{\Omega \cdot \text{cm}}$. When the applied voltage is close to the voltage required for the electrolysis of water, the conductivity G gains sharply up to about $10^{-1} \frac{1}{\Omega \cdot \text{cm}}$.

Due to the high conductivity W and the relatively high resistance of the electrodes Ra and Rb , the nonuniform behavior of the

Sample1 is more evident than that of the Sample2.

The experimental results of the voltage measurements and the electromechanical response of the Sample1 are depicted in Figure 4 and Figure 5 respectively.

The simulations of the Sample1 are given in Figure 16. The graphs demonstrate that voltage increases rapidly close to the input contacts and more slowly further away from the input contacts (Fig. 16.-A).

It is not possible to measure directly the distribution of electric current through the sheet. This data can be only derived from the simulations, using the equation (17). The distribution of current depicted in Figure 16.-B produces the bending motion of the sample depicted in Figure 16.-C. The graph exhibits that the actuator moves sharply only close to the input contacts. The noticeably weaker change of the curvature of the free end appears after a short delay. The behavior of the voltage and the flexure are rather similar to the parameters obtained by the measurements of a real actuator. They are presented in Figures 4 and 5 respectively.

The Sample1 exhibits insistent back-relaxation. As seen from Figure 5, in a half second after the beginning of the input pulse already. As we have no model for relaxation yet, we give here only the graphs for our case A - the step voltage is applied to the input of the initially discharged actuator.

The Sample2 is an ionic liquid containing IPMC made of 0.18 mm thick Nafion membrane. It is covered by a thin layer of RuO₂ powder and 20 nm gold foil electrodes glued to the ionomer with the dilution of Nafion. This material is intended to work in air. The conductivity of the surface of the gold electrodes of that material is very high, however the poor conductivity of the RuO₂ layer between the gold foil and the ionomer causes a high value of W . The large surface area of the RuO₂ powder supposedly creates large pseudocapacitance of the IPMC material. The ionic liquid used was EMITf and the cations introduced to the polymer were Li⁺.

Due to the pure conductivity of the RuO₂ layer between the gold electrode and the ionomer the ionic current inside the ionomer cannot grow fast. For that reason the voltage drop along the electrodes is imperceptible and the IPMC has nearly a constant bending radius as depicted in simulations in Figure 13. As

electric current between the electrodes cannot grow, this IPMC is slow. It gains its maximal flexure in minutes.

Sample2 bends slowly with an almost uniform bending radius over its full length. During the pulse the voltage along the sample is near to the uniform distribution, so that the voltage drop occurs on the conductivity W .

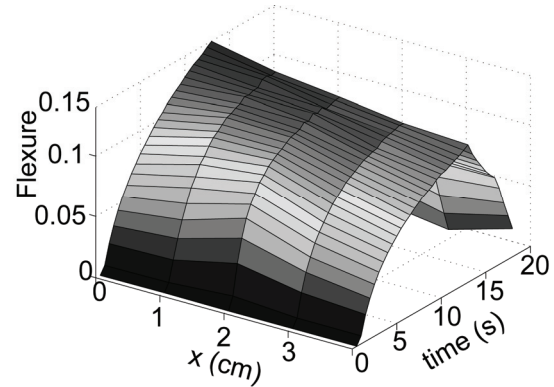


Figure 13. Measured mechanical response of Sample2.

The simulations of the charge, calculated according to (22) in the course of applied voltage and in the course of relaxation after the shorting of the input contacts are depicted in Figure 17.

The distribution of current between the surface electrodes is depicted in Figure 17-B. In contrast to the Sample 1 where the current peaked only for a very short time near the contacts creating non-uniform bending, the current of the Sample 2 is several orders of magnitudes weaker, but remains almost uniform along its full length for a long time, thereby producing uniform bending.

6.2. The behavior of actuators of different lengths

The length L of the IPMC actuators is one of the parameters of the model. According to the equations (22), (13) and (14) the transient behavior of the IPMC actuators is different in for the actuators having different length. The transient bending movement of a shorter actuator is not just similar to the first part of the longer one. In order to compare the transient bending behavior of the actuators of different lengths, we recorded some experiments of the bending movement of a strip of an IPMC, cut it shorter, and repeated the experiment. This method ensures that the electrical parameters of the strips are the same.

The driving signal of the is a 2V rectangular pulse for all the experiments. The overlays of a

series of frames are represented in Figure 18. It is clearly visible that the bending of the long actuator is inert and weak (Figure 18-A), while the bending of the the free tip of the almost twice shorter actuator (Figure 18-C) is much sharper and higher.

The photos of the strips of the IPMC are depicted in Figure 14. The IPMC material used was Musclesheet™ provided by Biomimetics Inc in 2004. The parameters of the strips are given in Table1 as the *Sample3*

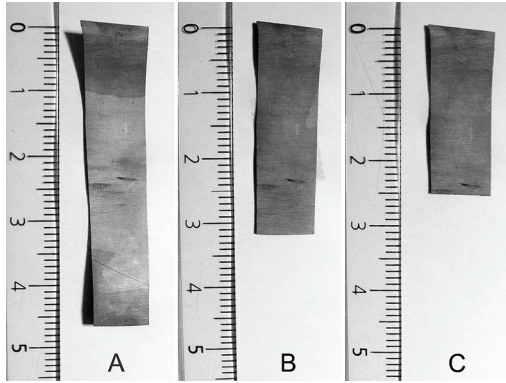


Figure 14. IPMC actuators of different lengths. A short slice is cut off from the same piece of IPMC in order to obtain the next one.

The simulated transient bending movements of the actuators of different lengths provided according to the equation (22) are depicted in Figure 15. The graphs exhibit that the amplitude of bending of the shorter actuator is higher and it is gained earlier than that of the longer actuators.

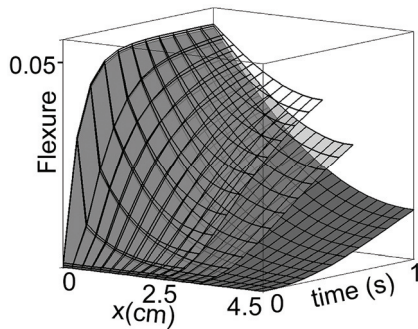


Figure 15. Simulated transient behavior of the IPMC actuators of different lengths made of the same IPMC material, drawn in the similar scale.

6.3. Quantitative validation of the model

6.3.1. Determination of the empiric constant Υ

As explained above, the flexure of an actuator at any location is proportional to the charge carried over at that particular location. The coefficient for the bending effect of the charge Υ (see (1)) is the only empirical constant in the model. It is reasonable to assume that Υ is constant all over the actuator if the experiments are done within a short period of time (i.e. the hydration level of the sample does not change considerably). With this assumption, we can identify Υ for the specific actuator for an arbitrary $k(x,t)$, and use the obtained value for the remaining points of the surface or even in the subsequent experiments. For model validation, the parameter Υ can be determined by comparing the experimental graph $k(x,t)$ and the simulated graph $q(x,t)$ of the mechanical response of the actuator $a k(x,t)$. The obtained value holds for the whole actuator for a while, as long as the material will not get mechanically exhausted.

6.3.1 Error estimation

There are two sets of parameters that are determined experimentally, both possible sources of measurement errors:

1. the determination of the angles of the bending, see Section 2 and Figure 3 ;
2. the estimation of the electrical parameters Ra , Rb , G , W and C of the material, see Section 5.

As the description of the shape of the actuator in time-domain is obtained by image processing, we should estimate the error of bending angles from the pixel sizes of the image of the actuator. Due to the setup of our camera and optics the width of the image of the actuator is as few as 1-2 pixels. For a segment of 60 pixels long, the largest error of the angle is $2/60 = \pm 8\%$. This error is not cumulative as each segment is treated separately. The smaller the segment is, the better it describes the shape of the actuator, but the larger is the measurement error.

The estimation of the electrical parameters of the materials was performed by a series of measurements (at least 200 each), and by averaging over the measurements. The standard deviation of the measurements was $<5\%$ for all cases. When the measurements were performed

at low voltages and electric currents, the results did not depend on the actual values of the voltages and currents.

6.3.3. Validation of the model with error estimates.

As described above, the largest measurement error comes from the measurements of the bending angles. In order to validate the model quantitatively we depict the error corridor of the angle measurements and the simulated results with the obtained electrical parameters on the same diagram. Figure 19 shows results for this comparison for the Samples 1 and 2. The arrow shows the conditions at which the coefficient Υ is determined: $x=0, t=0.8s$ for Sample1 and $x=0, t=8s$ for Sample2.

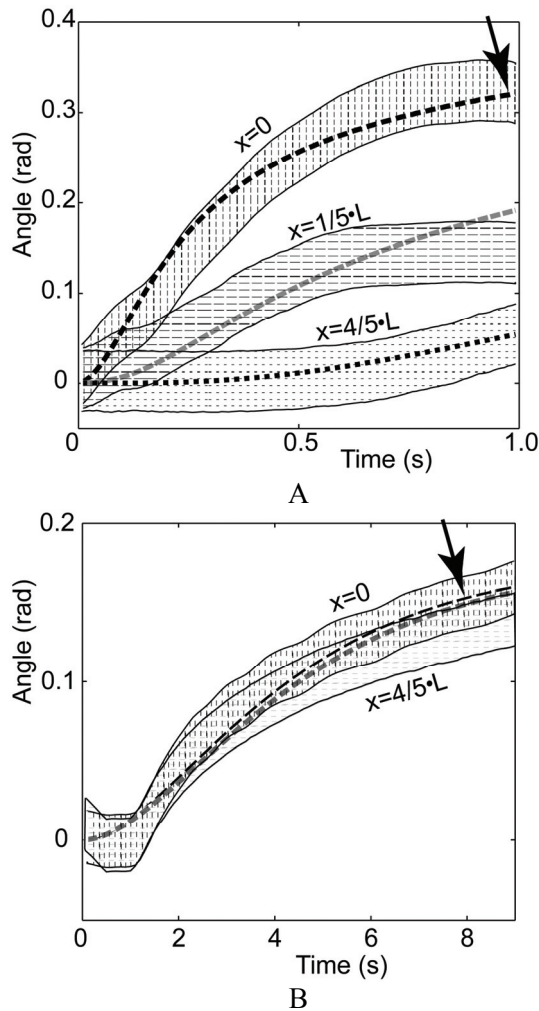


Figure 19. Comparison of the experimental and simulated results. A – Sample1, B – Sample2. The diagrams represent the error corridors of the measured flexure at different positions in conjunction with the simulated graphs (dashed lines).

We have chosen to identify Υ at the contacts of the actuator where we presume that the possible measurement error is smallest because of the large deflection angle. We found that $\Upsilon = 0.28 / 0.019 = 14.7$ for Sample 1 and $\Upsilon = 0.13 / 0.02 = 6.5$ for Sample 2. For Sample 3 (see Figures 15 and 18) $\Upsilon = 5.4$.

The diagrams indicate that even if the electrical parameters vary in the range of the measurement error, the simulated graph remains in the error corridor of the measured angles as long as the back-relaxation will not occur. The dissimilarity between the simulated and experimental behavior is clearly recognizable e.g. in Figure 19-A, where the actuator relaxes at the position $x = 1/5 \cdot L$ at $t > 0.8$ seconds. As your model does not describe back-relaxation, the dissimilarity increasing in time starts to become evident.

7. DISCUSSION

The presented distributed one-dimensional model of an IPMC consists of a number of lumped models coupling them with a spatial parameter – a generally uneven distribution of voltage caused by the resistance of the electrodes. It shows a good correlation with the experimental data obtained from the measurements conducted with the different IPMC materials. Its advantages with respect to the previous models are:

- it permits modeling the non-uniform flexure of the IPMC actuator in spatial and time domain.
- it permits modeling large flexure of the actuator or sensor.
- it takes into account the real measurable parameters of the material – resistance of the electrodes and capacitance and with respect to the previously developed models does not reduce it to a uniform lumped model;
- it is scalable, i.e. the length of the actuator is one of the parameters of the model;
- the values of the measurable parameters - the capacitance of the material, the resistance of the electrodes and the length - may vary on a large scale.

The model described in the current paper gives the analytical solution for the free bending of the IPMC actuators only. It does not take into account the mechanical parameters of IPMC membranes, for example the viscoelasticity of polymer membranes, the blocking force

produced by the IPMC actuator, inertia, etc. Presumably the combination of the electrical distributed model and the theory of mechanics of multilayer elastic thin films would give a result, capable to express the force produced by an arbitrary segment of the actuator.

The described analytical model presumes that the electrical parameters of the material R_a , R_b , G , W and C are invariant. This presumption is valid at low voltages only. Measuring the resistances G and W with voltage pulses of various amplitudes gives a well determined relation between the values of the resistors and the voltage. When the amplitude of the voltage approaches to the voltage required for water electrolysis, the resistances G and W decrease fast due to the electrode reactions, reaching very low values. In this case the analytical equations given in Section 4 are not tenable any more.

IPMC materials are also known to have sensor properties, When the material is

mechanically deformed, it generates a weak voltage between the faces of the IPMC sheet due to the change of the concentration of ions. According to (2) voltage at output contacts depends on time and distance between the bending area and the output. If the deformation is continuous or distributed, the values of $U(x,t)$ should be superpositioned. Verification of the proposed model for IPMC sensors is a subject of our future work.

8. ACKNOWLEDGEMENTS

This work has been supported by Estonian Ministry of Education, European Science Foundation, Estonian Science Foundation grants 6765, 6785 and 6763 and by Estonian Information Technology Foundation.

Table 1. The parameters of the samples

sample	dimensions (mm)	thickness of ionomer (μm)	R_a ($\frac{\Omega}{\text{cm}}$)	R_b ($\frac{\Omega}{\text{cm}}$)	W ($\frac{1}{\Omega\cdot\text{cm}}$)	G ($\frac{1}{\Omega\cdot\text{cm}}$)	C ($\frac{F}{\text{cm}}$)	cations
1.	10 x 35	250	9	5	1	0.0005	0.02	Li^+
2.	10 x 35	180	0.5	0.5	0.015	0.0001	0.02	Li^+
3.	8 x XX	180	3	1.5	0.5	0.0015	0.05	Li^+

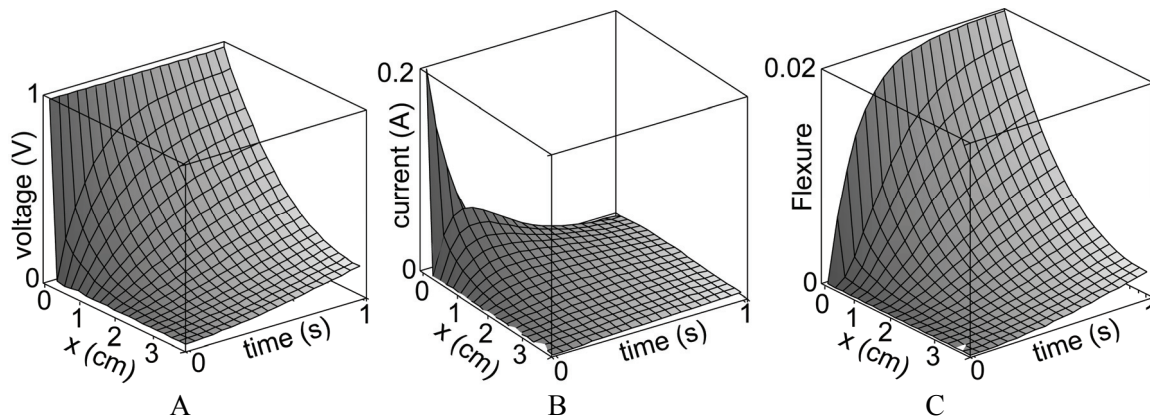


Figure 16. Simulations of Sample1. A – voltage, B – current, C – charge.

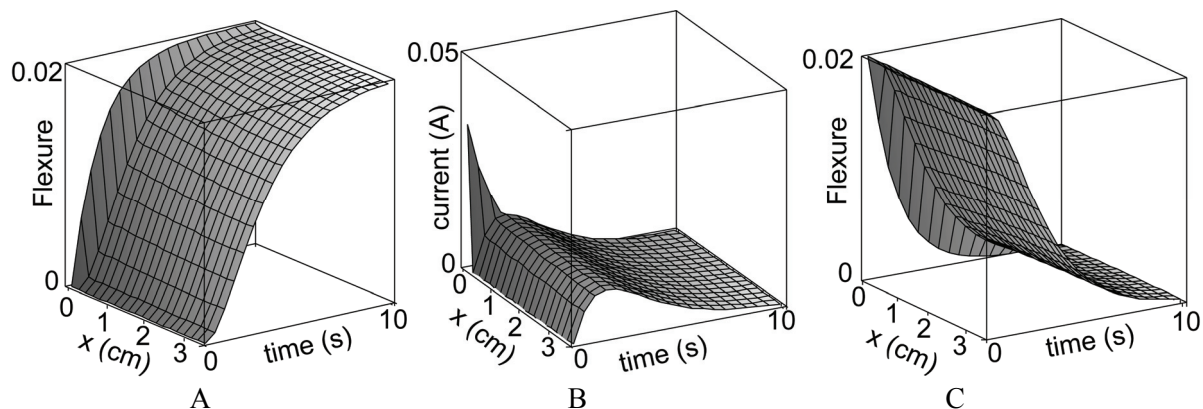


Fig. 17. Simulations of Sample2. A - charge during the step voltage input; B - current during voltage input; C - charge during relaxation.

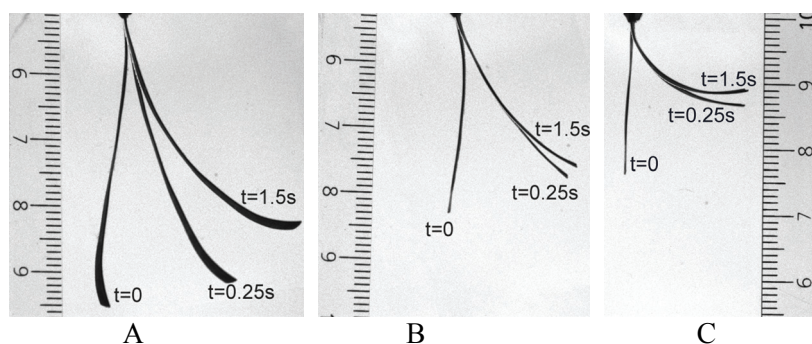


Fig. 18. Overlay of a series of frames of different time instants of 3 experiments with actuators made of the same material - Sample3. The time instants of the frames are the initial position ($t=0s$); in the middle of the bending ($t=0.25s$); and the steady position ($t=1.5s$).

REFERENCES

- Asaka, K. and Oguro, K. 2000. „Bending of Polyelectrolyte Membrane-Platinum Composites by Electric Stimuli. Part II, Response Kinetics”, *J. Electroanal. Chem.*, 480:186-198
- Bandopadhyaya, D. et al. 2006. “Active vibration suppression of a flexible link using ionic polymer metal composite,” *Proc. IEEE Conference on Robotics, Automation and Mechatronics*, 1-6.
- Bao, X. et al. 2002. “Measurements and Macro Models of Ionomeric Polymer-Metal Composites (IPMC),” *EAPAD Conference 2002, Proc. SPIE (4695):286-293.*
- Berry, B.S. and Pritchett, W.C. 1984 “Bending-cantilever method for the study of moisture swelling in polymers,” *IBM J. Res. Develop.*, 28(6):662-667
- Bonomo, C. et al. 2007. „A nonlinear model for ionic polymer metal composites as actuators”, *Smart Mater. Struct.* 16:1-12.
- Jung, K. et al. 2003. “Investigations on actuation characteristics of IPMC artificial muscle actuator,” *Sensors and Actuators A: Physical*, 107(2):183–192.
- Kanno, R. et al. 1995. „Modeling of ICPF Actuator, Modeling of Electrical Characteristics” *Proc. IEEE 21st Intl Conf. On Industrial Electronics, Control, and Instrumentation*, 2:913-918.
- Kanno, R. et al. 1996 “Linear approximate dynamic model of an ICPF actuator”, *Proc. IEEE Intern. Conf. on Robotics and Automation*, 1:219-225.
- Kothera, C.S. 2005. “Characterization, Modeling, and Control of the Nonlinear Actuation Response of Ionic Polymer Transducers”, Ph.D. dissertation, Dept. of Mechanical Engineering, Virginia Tech.
- Kreyszig, E. 2006. “Advanced Engineering Mathematics”, 9th Ed., Wiley.
- Mallavarapu, K. and Leo, D. 2001. “Feedback Control of the bending response of ionic polymer actuators,” *Journal of Intelligent Material Systems and Structures*, 12(3):143–155.
- Nemat-Nasser, S. and Thomas, C.W. 2004. “Ionomeric polymer-metal composites”, in: Bar-Cohen, Y. (ed.), “Electroactive Polymer (EAP) Actuators as Artificial Muscles. Reality, Potential, and Challenges,” SPIE Press, Washington.
- Newbury, K. and Leo, D. 2003. „Linear Electro-mechanical Model of Ionic Polymer Transducers – Part I: Model Development”, *Journal of Intelligent Material Systems and Structures*, 14(6):333–342.
- Punning, A. and Jalviste, E. 2009. “Analytical Solution for Voltage-Step Response of Lossy Distributed RC Lines”, *IEEE Transactions on Microwave Theory and Techniques*. *Accepted for publishing, scheduled to appear in the February, 2009 issue of the journal.*
- Powers, D.L. 2006. “Boundary value Problems and Partial Differential Equations”, Elsevier.
- Richardson, R.C. et al. 2003. “Control of ionic polymer metal composites,” *IEEE/ASME Transactions on Mechatronics*, 8(2):245–253.
- Sadeghipour, K. et al. 1992. “Development of a novel electro-chemically active membrane and “smart” material based vibration sensor/damper,” *Smart Materials and Structures*, 1:172–179.

- Shahinpoor, M. 2003. "Ionic polymer-conductor composites as biomimetic sensors, robotic actuators and artificial muscles – a review", *Electrochimica Acta* 48:2343-2353
- Shahinpoor, M. and Kim, K.J. 2005. "Ionic polymer-metal composites: IV. Industrial and medical applications," *Smart Materials and Structures*, 14:197-214.
- Tadokoro, S. et al. 2004. "Modeling IPMC for Design of Actuation Mechanism" in: Bar-Cohen, Y. (ed.), "Electroactive Polymer (EAP) Actuators as Artificial Muscles. Reality, Potential, and Challenges," SPIE Press, Washington.
- Timoshenko, S.P. 1925. "Analysis of bi-metal thermostats," *J. Opt. Soc. Am.* 11:, 233-255.
- Yim, W. et al. 2006. "Dynamic Modeling of Segmented Ionic Polymer Metal Composite (IPMC) Actuator," *Proc. IEEE/RSJ Int. Conf. on Intelligent Robots and Systems* 5459-5464.